

# Uncertainty in non-linear long-term behavior and buckling of shallow concrete-filled steel tubular arches

\*X. Shi<sup>1</sup>, W. Gao<sup>1</sup>, Y.L. Pi<sup>1</sup>

<sup>1</sup>School of Civil and Environment Engineering, The University of New South Wales, Sydney,  
NSW 2052, Australia.

\*Corresponding author: shixue1985@hotmail.com

**Abstract:** This paper presents a theoretical analysis for the non-deterministic time-dependent non-linear behavior of shallow concrete-filled steel tubular (CFST) arches with interval parameters under a sustained uniform load. The change ranges of the final shrinkage strain and final creep coefficients of concrete core are derived from experimental results. The virtual work method is used to establish the differential equations of equilibrium for the time-dependent behavior and buckling analyses of shallow CFST arches, and the age-adjusted effective modulus method is adopted to model the creep behavior of the concrete core. Analytical solutions of the interval time-dependent displacements and internal forces of shallow CFST arches are derived. The lower and upper bounds of structural responses are determined. Comparisons of the interval analytical solutions with the interval finite element results show that the analytical solutions of the present study are accurate.

**Keywords:** CFST arches, interval analysis, creep, shrinkage

## 1. Introduction

Applications of concrete filled steel tubular (CFST) arches are increasing in engineering structures, particularly in bridge constructions. The visco-elastic effects of creep and shrinkage of concrete core are inevitable in the long term for CFST arches. When a CFST arch is subjected to a sustained load, the creep of the concrete core will lead to the increase of its deformations with time and the deformations may be significant, while the shrinkage strain may also develop even when the arch is not subjected to any load [B.C. Chen 2000]. Hence, an investigation of significant effects of creep and shrinkage of the concrete core on the time-dependent structural behavior of CFST arches is much needed.

However, it is noted that the creep coefficient obtained from tests vary significantly from one experiment to another. Very different predictions of the time-dependent behavior of CFST columns have been reported in different studies. This shows that the uncertainties of creep and shrinkage of the concrete core do exist. To predict the long-term behavior of CFST columns reasonably, these uncertainties have to be considered.

In this paper, intervals are adopted to represent the uncertainties. This paper, therefore,

aims to investigate the interval time-dependent non-linear behavior and buckling of shallow CFST arches under a uniform radial load, to derive analytical solutions for their time-dependent non-linear deformations, internal forces and buckling, and to determine their structural life time prior to the buckling. To investigate the effects of the creep and shrinkage of concrete core, it is important to use an efficient and accurate method to describe the creep and shrinkage of concrete. [Pi et al. (2002), Pi et al. (2007)] It is known that a number of methods have been proposed and used for the creep and shrinkage of the concrete. Among these methods, the age-adjusted effective modulus method recommended by ACI Committee-209 and Australia design code for the concrete structures AS3600 are commonly considered to be efficient and accurate in evaluating the time-dependent behavior of the concrete and it could conveniently be incorporated into the structural analysis [ACI Committee 209 1982]. Algebraic formulas used in this method can be effective and practicable in modeling creep and shrink-age of concrete core, so the age-adjusted effective modulus method is used in this investigation.

## 2. Interval nonlinear elastic analysis of long-term behavior of shallow CFST arches

To predict the long-term performance, interval constitutive model considering creep and shrinkage of the CFST column needs to be established. The basic assumptions adopted for the interval long-term linear elastic analysis of CFST columns in this paper are: (1) deformations of CFST arch are elastic and satisfy the Euler-Bernoulli hypothesis, i.e. the cross-section remains plane and perpendicular to the arch axis during deformation; (2) the dimensions of the cross-section are much smaller than the length and radius of the arch so that the arches are sufficiently slender; and (3) the cohesion and adhesion of two different material components are fully bonded.

To account for the non-linearity resulted from creep and shrinkage of the concrete core, the derivation of the differential equations of equilibrium for shallow CFST arches need to consider non-linear longitudinal normal strain-displacement relationship and the non-linear longitudinal normal strain  $\varepsilon$  of an arbitrary point in the cross-section of shallow CFST arches can then be expressed as [Pi et al 2002]

$$\varepsilon = \tilde{w} - \tilde{v} + \frac{1}{2}(\tilde{v}')^2 - \frac{y\tilde{v}''}{R} \quad (1)$$

According to the third assumption, the deformations of each component should be compatible with each other, so their membrane strains and also the strains at the interface are identical. However, due to different Young's moduli and the effects of creep and shrinkage in concrete core, the stress  $\sigma_s$  in the steel tube and the stress

$\sigma_c$  in the concrete core are different and they are given by

$$\sigma_c = E_{ec}(\varepsilon + \varepsilon_{sh}) = E_{ec}(u' + \varepsilon_{sh}) \quad (2)$$

and

$$\sigma_s = E_s \varepsilon \quad (3)$$

where  $E_{ec}$  is the age-adjusted effective modulus of concrete,  $\varepsilon_{sh}$  is the shrinkage strain of concrete and can be given by AS3600 [AS3600 2001]

$$\varepsilon_{sh}(t) = \frac{\varepsilon_{shfinal}}{35+t} \cdot t \quad (4)$$

where  $t$  is the loading time,  $\varepsilon_{shfinal}$  is the final shrinkage strain of concrete when  $t \rightarrow \infty$ .

$E_{ec}$  can be calculated by

$$E_{ec}(t, \tau_0) = \frac{E_c}{1 + \chi(t, \tau_0)\varphi(t, \tau_0)} \quad (5)$$

where  $\tau_0$  is the age at loading,  $\chi(t, \tau_0)$  is the aging coefficient and  $\varphi(t, \tau_0)$  is the creep coefficient that can be expressed as

$$\varphi(t, \tau_0) = \left[ \frac{(t - \tau_0)^{0.6}}{10 + (t - \tau_0)^{0.6}} \right] \cdot \varphi_{final} \quad (6)$$

where  $\varphi_{final}$  is the final creep coefficient when  $t \rightarrow \infty$ . The aging coefficient  $\chi(t, \tau_0)$  can be expressed as

$$\chi(t, \tau_0) = 1 - \frac{(1 - \chi^*)(t - \tau_0)}{20 + (t - \tau_0)} \quad (7)$$

where

$$\chi^* = \frac{k_1 \tau_0}{k_2 + \tau_0} \quad (8)$$

with

$$k_1 = 0.78 + 0.4e^{-1.33\varphi_{\infty,7}} \quad (9)$$

$$k_2 = 0.16 + 0.8e^{-1.33\varphi_{\infty,7}} \quad (10)$$

$$\varphi_{\infty,7} = \varphi_{final} t_0^{0.118} / 1.25 \quad (11)$$

The differential equations for the long-term analysis of a CFST arch can be obtained using a virtual work method. When the virtual work principle is used for the long-term equilibrium of the CFST arch, it can be stated as requiring that the functional

$$\int_{-\Theta}^{\Theta} [-NR(\delta\tilde{w}' - \delta\tilde{v} + \tilde{v}'\delta\tilde{v}') - M\delta\tilde{v}''] - qR^2\delta\tilde{v}d\theta = 0 \quad (12)$$

where the axial compressive force  $N$  is given by

$$N = -\int_{A_s} \sigma_s dA - \int_{A_c} \sigma_c dA = -(A_s E_s + A_c E_{ec}^I)[\tilde{w}' - \tilde{v}' + \frac{1}{2}(\tilde{v}')^2] - A_c E_{ec}^I \varepsilon_{sh}^I \quad (13)$$

and the bending moment is given by

$$M = \int_{A_s} \sigma_s y dA + \int_{A_c} \sigma_c y dA = (E_s I_s + E_{ec} I_c) \frac{\tilde{v}''}{R} \quad (14)$$

in the axial direction:

$$N' = 0 \quad (15)$$

in the radial direction:

$$-M'' + NR\tilde{v}'' + NR - qR^2 = 0 \quad (16)$$

and leads to the static boundary conditions for pin-ended arches as

$$M = 0 \text{ at } \theta = \pm\Theta$$

From Eq.(15), the axial compressive force N is constant along the arch axis. Substituting the constant axial compressive force N and the expression for M given by Eq.(14) into Eq.(16) leads to

$$\frac{\tilde{v}^{iv}}{(\mu_e^I)^2} + \tilde{v}'' = P \quad (17)$$

where  $\mu_e^I$  is a time-dependent dimensionless axial force parameter defined by

$$\mu_e^I = \left[ \sqrt{\frac{NR^2}{E_s I_s + E_{ec} I_c}}, \sqrt{\frac{\bar{N}R^2}{E_s I_s + E_{ec} I_c}} \right] \quad (18)$$

and P is a dimensionless load defined by

$$P^I = \frac{qR - N^I}{N^I} \quad (19)$$

By using the kinematic boundary conditions and the static boundary conditions and the kinematic boundary conditions, the solutions of Eq.(17) can be obtained as

For Pin-ended:

The radial displacement can be expressed as

$$\tilde{v}^I = \left[ \frac{\bar{P}}{\mu_e^2} \left\{ \frac{\cos(\mu_e \theta) - \cos(\mu_e \Theta)}{\cos(\mu_e \Theta)} + \frac{1}{2} [(\mu_e \theta)^2 - (\mu_e \Theta)^2] \right\}, \frac{P}{\mu_e} \left\{ \frac{\cos(\bar{\mu}_e \theta) - \cos(\bar{\mu}_e \Theta)}{\cos(\bar{\mu}_e \Theta)} + \frac{1}{2} [(\bar{\mu}_e \theta)^2 - (\bar{\mu}_e \Theta)^2] \right\} \right] \quad (20)$$

And the axial displacement can be expressed as:

Lower bound of axial displacement:

$$\begin{aligned} \tilde{w} = & \frac{(1 - \bar{P})\bar{P}\theta(\theta^2 - \Theta^2)}{6} + \frac{(1 + \bar{P})\bar{P}[\Theta \sin(\mu_e \theta) - \theta \sin(\mu_e \Theta)]}{\mu_e^3 \Theta \cos(\mu_e \Theta)} \\ & + \frac{\bar{P}^2 \theta}{\mu_e^2} \left[ 1 - \frac{\cos(\mu_e \theta)}{\cos(\mu_e \Theta)} \right] + \frac{\bar{P}^2 [\Theta \sin(\mu_e \theta) \cos(\mu_e \theta) - \theta \sin(\mu_e \Theta) \cos(\mu_e \Theta)]}{4\mu_e^3 \Theta \cos^2(\mu_e \Theta)} \end{aligned} \quad (21)$$

Upper bound of axial displacement:

$$\begin{aligned} \bar{w} = & \frac{(1-P)\bar{P}\theta(\theta^2 - \Theta^2)}{6} + \frac{(1+P)\bar{P}[\Theta \sin(\bar{\mu}_e \theta) - \theta \sin(\bar{\mu}_e \Theta)]}{\bar{\mu}_e^3 \Theta \cos(\bar{\mu}_e \Theta)} \\ & + \frac{(P)^2 \theta}{\bar{\mu}_e^2} \left[1 - \frac{\cos(\bar{\mu}_e \theta)}{\cos(\bar{\mu}_e \Theta)}\right] + \frac{P^2 [\Theta \sin(\bar{\mu}_e \theta) \cos(\bar{\mu}_e \theta) - \theta \sin(\bar{\mu}_e \Theta) \cos(\bar{\mu}_e \Theta)]}{4\bar{\mu}_e^3 \Theta \cos^2(\bar{\mu}_e \Theta)} \end{aligned} \quad (22)$$

For Fixed:

The radial displacement can be expressed as

Lower bound of radial displacement:

$$\bar{v} = \frac{\bar{P}}{\bar{\mu}_e^2} \left\{ \frac{(\bar{\mu}_e \Theta) [\cos(\bar{\mu}_e \theta) - \cos(\bar{\mu}_e \Theta)]}{\sin(\bar{\mu}_e \Theta)} + \frac{1}{2} [(\bar{\mu}_e \theta)^2 - (\bar{\mu}_e \Theta)^2] \right\} \quad (23)$$

Upper bound of radial displacement

$$\bar{v} = \frac{P}{\bar{\mu}_e^2} \left\{ \frac{(\bar{\mu}_e \Theta) [\cos(\bar{\mu}_e \theta) - \cos(\bar{\mu}_e \Theta)]}{\sin(\bar{\mu}_e \Theta)} + \frac{1}{2} [(\bar{\mu}_e \theta)^2 - (\bar{\mu}_e \Theta)^2] \right\} \quad (24)$$

And the axial displacement can be expressed as:

Lower bound of axial displacement:

$$\begin{aligned} \bar{w} = & \frac{(1-\bar{P})\bar{P}\theta(\theta^2 - \Theta^2)}{6} - \frac{(1+\bar{P})\bar{P}}{\bar{\mu}_e^2} \left[ \theta - \frac{\Theta \sin(\bar{\mu}_e \theta)}{\sin(\bar{\mu}_e \Theta)} \right] \\ & - \frac{\bar{P}^2 \theta \Theta}{\bar{\mu}_e \sin(\bar{\mu}_e \Theta)} \left[ \frac{3 \cos(\bar{\mu}_e \Theta)}{4} - \cos(\bar{\mu}_e \theta) \right] + \frac{\bar{P}^2 \Theta^2 \sin(\bar{\mu}_e \theta) \theta \cos(\bar{\mu}_e \theta)}{4\bar{\mu}_e \sin^2(\bar{\mu}_e \Theta)} \\ & + \frac{\bar{P}^2 \theta}{\bar{\mu}_e^2} \left[1 - \frac{\cos(\bar{\mu}_e \theta)}{\cos(\bar{\mu}_e \Theta)}\right] + \frac{\bar{P}^2 [\Theta \sin(\bar{\mu}_e \theta) \cos(\bar{\mu}_e \theta) - \theta \sin(\bar{\mu}_e \Theta) \cos(\bar{\mu}_e \Theta)]}{4\bar{\mu}_e^3 \Theta \cos^2(\bar{\mu}_e \Theta)} \end{aligned} \quad (26)$$

Upper bound of axial displacement:

$$\begin{aligned} \bar{w} = & \frac{(1-P)P\theta(\theta^2 - \Theta^2)}{6} - \frac{(1+P)P}{\bar{\mu}_e^2} \left[ \theta - \frac{\Theta \sin(\bar{\mu}_e \theta)}{\sin(\bar{\mu}_e \Theta)} \right] \\ & + \frac{P^2 \theta \Theta}{\bar{\mu}_e \sin(\bar{\mu}_e \Theta)} \left[ \frac{3 \cos(\bar{\mu}_e \Theta)}{4} - \cos(\bar{\mu}_e \theta) \right] + \frac{P^2 \Theta^2 \sin(\bar{\mu}_e \theta) \theta \cos(\bar{\mu}_e \theta)}{4\bar{\mu}_e \sin^2(\bar{\mu}_e \Theta)} \\ & + \frac{P^2 \theta}{\bar{\mu}_e^2} \left[1 - \frac{\cos(\bar{\mu}_e \theta)}{\cos(\bar{\mu}_e \Theta)}\right] + \frac{P^2 [\Theta \sin(\bar{\mu}_e \theta) \cos(\bar{\mu}_e \theta) - \theta \sin(\bar{\mu}_e \Theta) \cos(\bar{\mu}_e \Theta)]}{4\bar{\mu}_e^3 \Theta \cos^2(\bar{\mu}_e \Theta)} \end{aligned} \quad (27)$$

### 3. Interval finite element analyses

For interval buckling analysis, buckling load and equilibrium paths are sought by solving the equilibrium equation at each load increment. The equilibrium equation can be expressed as:

$$K_T^I \Delta u^I = \Delta P \quad (28)$$

At each load increment, perturbation method was employed to calculate the global

stiffness matrix. In the following, the effects of the beam axial force and bending are included. The creep coefficient and final shrinkage strain are considered as interval parameters. Using the first-order Taylor expansion and the interval arithmetic operations [Rao et al. 1997], the interval stiffness coefficients of the beam-column element can be obtained as

$$\begin{aligned}
& K_{Ti}(\varphi_{final}^I, \varepsilon_{shfinal}^I) = \\
& K_{Ti}(\varphi_{final}^c, \varepsilon_{shfinal}^c) + \frac{\partial K_{Ti}(\varphi_{final}^c, \varepsilon_{shfinal}^c)}{\partial \varphi_{final}^c} (\varphi_{final}^I - \varphi_{final}^c) \\
& + \frac{\partial K_{Ti}(\varphi_{final}^c, \varepsilon_{shfinal}^c)}{\partial \varepsilon_{shfinal}^c} (\varepsilon_{shfinal}^I - \varepsilon_{shfinal}^c) \quad (29) \\
& = K_{Ti}(\varphi_{final}^c, \varepsilon_{shfinal}^c) + \frac{\partial K_{Ti}(\varphi_{final}^c, \varepsilon_{shfinal}^c)}{\partial \varphi_{final}^c} \Delta \varphi_{final} e_{\Delta} + \\
& \frac{\partial K_{Ti}(\varphi_{final}^c, \varepsilon_{shfinal}^c)}{\partial \varepsilon_{shfinal}^c} \Delta \varepsilon_{shfinal} e_{\Delta}
\end{aligned}$$

where  $i$  denotes the number of elements,  $\varphi_{final}^c = \frac{\overline{\varphi_{final}} + \underline{\varphi_{final}}}{2}$ ,  $\Delta \varphi_{final} = \frac{\overline{\varphi_{final}} - \underline{\varphi_{final}}}{2}$ ,

$\varepsilon_{shfinal}^c = \frac{\overline{\varepsilon_{shfinal}} + \underline{\varepsilon_{shfinal}}}{2}$ ,  $\Delta \varepsilon_{shfinal} = \frac{\overline{\varepsilon_{shfinal}} - \underline{\varepsilon_{shfinal}}}{2}$ ,  $e_{\Delta} = [-1, 1]$ . From Eq. (29), it can be

easily observed that the stiffness is the function of the creep coefficient and final shrinkage strain.

The interval global stiffness matrix of the structure is assembled using the following equation

$$\begin{aligned}
& K_T(\varphi_{final}^I, \varepsilon_{shfinal}^I) = \sum_{i=1}^n K_{Ti}(\varphi_{final}^I, \varepsilon_{shfinal}^I) \\
& = K_T(\varphi_{final}^c, \varepsilon_{shfinal}^c) + \sum_{i=1}^n \left[ \frac{\partial K_{Ti}(\varphi_{final}^c)}{\partial \varphi_{final}^c} \Delta E + \frac{\partial K_{Ti}(\varepsilon_{shfinal}^c)}{\partial \varepsilon_{shfinal}^c} \Delta E \right] e_{\Delta} \quad (30)
\end{aligned}$$

Then the interval static equation of equilibrium in the interval finite element system becomes

$$K_T(\varphi_{final}^I, \varepsilon_{shfinal}^I) \Delta(U^c + \Delta U e_{\Delta}) = \Delta P \quad (31)$$

yields

$$\Delta U = \left| K_T^{-1}(\varphi_{final}^c, \varepsilon_{shfinal}^c) \left[ \sum_{i=1}^n \left( \frac{\partial K_{Ti}(\varphi_{final}^c)}{\partial \varphi_{final}^c} \Delta E + \frac{\partial K_{Ti}(\varepsilon_{shfinal}^c)}{\partial \varepsilon_{shfinal}^c} \Delta E \right) e_{\Delta} \right] \right| U^c \quad (32)$$

To overcome the computational difficulties caused by the singularity of the tangent stiffness matrix at the limit points on the equilibrium path, the interval incremental-iterative solution is introduced for this study.

The incremental-iterative equilibrium equation at time  $t$  and iterative step  $i$  can be expressed as

$${}^t[K_T]_i^I {}^t \Delta U_i^I = {}^t \Delta P(u) + {}^{t-\Delta t} \Delta P_r \quad (33)$$

where the subscript  $i$  denotes the iterative cycle, the superscript  $t$  denotes the load step,  ${}^t \Delta P(u)$  is the incremental external forces at time  $t$  and  ${}^{t-\Delta t} \Delta P_r$  is the unbalance forces at time  $t - \Delta t$ .

#### 4. Model validation and discussions

**4.1 Determination of intervals for the final shrinkage strain and creep coefficient**  
the interval of the final shrinkage strain and creep coefficient of their concrete cores can be derived from other researchers' [Uy.B 2001] test results as  $\varepsilon_{shfinal} = [43.5, 340]$

and  $\varphi_{final} = [0.5, 1.7]$  respectively, which are used in this study. It can be expected that the results obtained by the interval models proposed in this paper will contain these experimental results; in other words, the experimental results will fall into the interval bounds produced by the proposed models.

The creep coefficients determined by Uy [Uy.B 2001] is adopted to compare with the results obtained by the interval analytical model developed in this paper, which are illustrated in Figs. 1. Similarly, the total shrinkage strain determined by Uy is compared with the results given by the proposed interval model in Fig. 2. It can be easily seen that the results produced by the proposed model contain these experimental results as predicated. The bounds can be further updated if more experimental results available. These bounds will be useful for the future experimental investigations and design.

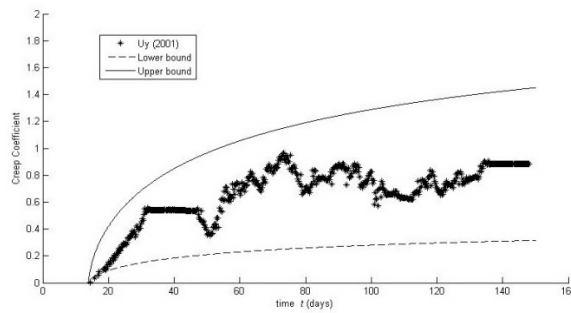


**Fig.1 Comparison of creep coefficient**

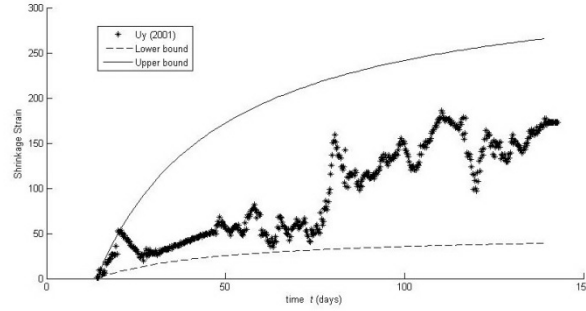


**Fig.2 Comparison of shrinkage strain**

The typical long-term nonlinear responses of pin-ended and fixed shallow CFST arches under a sustained uniform radial load are compared in Figs. 3 with their linear counter parts as the variations of the dimensionless central radial displacements  $v_c / v_{c,15}$  and the dimensionless axial displacements is  $w_{\theta/2} / w_{\theta/2,15}$  at the quarter point with time  $t$ , where the Young's moduli of the steel and concrete were assumed as  $E_s=200$  GP and  $E_c=30$  GPa. A circular cross-section with outer and inner radii:  $R=250$  mm and  $r=240$  mm was used in the investigation. The span of the arch was  $L=15$  m and the rise-to-span ratio of the pin-ended and fixed CFST arch were  $f/L=1/12$ , respectively.

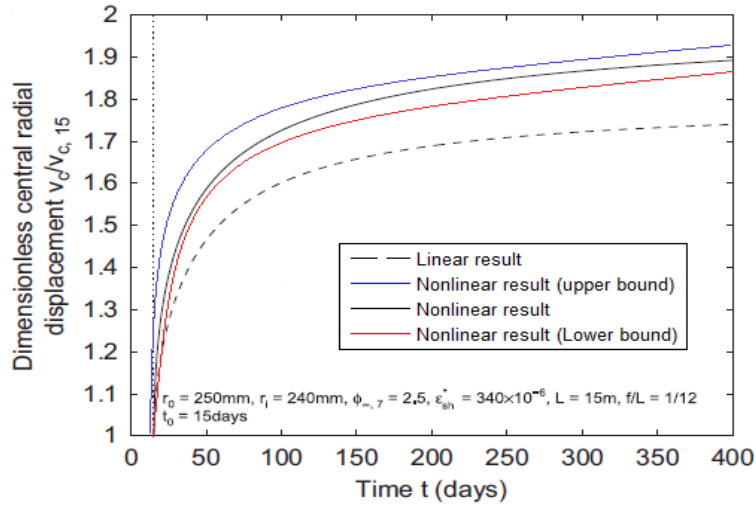


**Figure 3 Interval radial displacements**

## 5. Conclusions

This paper presents a theoretical study on the uncertain long-term and buckling analysis of shallow concrete-filled steel tubular arches subjected to a sustained uniform radial load. An interval analytical model based on the algebraically tractable age-adjusted effective modulus method is proposed to describe the time-dependent behavior of concrete in CFST arches. Non-linear analytical solutions for the time-dependent displacements and internal actions were derived. It has been found that creep and shrinkage of concrete core have significant effects on the

time-dependent non-linear deformations, internal forces and buckling behavior of shallow CFST arches.

An interval finite element was developed to describe the long-term behavior and analysis buckling. The buckling load or buckling time can be evaluated using this model. The result is compared with analytical results; it could be found it shows a good agreement. In the future, the proposed models will be further developed to analyze other types of CFST structures accounting for the uncertainties in their material and geometric properties.

## Reference

- ACI Committee 209, Prediction of Creep, Shrinkage and Temperature Effects in Concrete Structures, American Concrete Institute (ACI), Detroit, 1982.
- AS3600, Australian Standard: Concrete Structures, Standard Association of Australia, Sydney, 2001
- B.C. Chen, Experimental study on mechanical behaviors of concrete-filled steel tubular rib arch under in-plane loads, *Engineering Mechanics* **17** 44–50.
- Rao SS, Berke L. Analysis of uncertain structural systems using interval analysis. *AIAA J* 1997;**35**(4):727±35.
- Uy. B. ‘Static long-term effects in short concrete-filled steel box columns under sustained loading.’ *ACI Struct. J.*, **98**, 96–104.
- Y.-L. Pi, M.A. Bradford, B. Uy, In-plane stability of arches, *International Journal of Solids and Structures* **39** (2002) 105–125.
- Y.-L. Pi, M.A. Bradford, F. Tin-Loi, Nonlinear analysis and buckling of elastically supported circular shallow arches, *International Journal of Solids and Structures* **44** (7–8) (2007) 2401–2425.